nature physics

ARTICLES

PUBLISHED ONLINE: 9 MARCH 2015 | DOI: 10.1038/NPHYS3265

Snapshots of the retarded interaction of charge carriers with ultrafast fluctuations in cuprates

S. Dal Conte[1*†], L. Vidmar[2,3*†], D. Golež[3], M. Mierzejewski[4], G. Soavi[1], S. Peli[5,6], F. Banfi[5,7], G. Ferrini[5,7], R. Comin[8,9], B. M. Ludbrook[8,9], L. Chauviere[8,9,10], N. D. Zhigadlo[11], H. Eisaki[12], M. Greven[13], S. Lupi[14], A. Damascelli[8,9], D. Brida[1,15], M. Capone[16], J. Bonča[3,17], G. Cerullo[1] and C. Giannetti[5,7*]

One of the pivotal questions in the physics of high-temperature superconductors is whether the low-energy dynamics of the charge carriers is mediated by bosons with a characteristic timescale. This issue has remained elusive as electronic correlations are expected to greatly accelerate the electron–boson scattering processes, confining them to the very femtosecond timescale that is hard to access even with state-of-the-art ultrafast techniques. Here we simultaneously push the time resolution and frequency range of transient reflectivity measurements up to an unprecedented level, enabling us to directly observe the ∼16 fs build-up of the effective electron–boson interaction in hole-doped copper oxides. This extremely fast timescale is in agreement with numerical calculations based on the *t*–*J* model and the repulsive Hubbard model, in which the relaxation of the photo-excited charges is achieved via inelastic scattering with short-range antiferromagnetic excitations.

After almost 30 years of intensive experimental and theoretical efforts to understand the origin of high-temperature superconductivity in copper oxides, a consensus about the microscopic process responsible for the superconducting pairing is still lacking. The large Coulomb repulsion $U \gg 1$ eV between two electrons occupying the same lattice site is believed to have fundamental consequences for the normal state of these systems[1], and it is not clear whether a BCS-like bosonic glue that mediates the electron interactions and eventually leads to pairing can still be defined[2–4]. The fundamental issue can be reduced to the question whether the electronic interactions are essentially unmediated and instantaneous, or whether the low-energy physics, including superconductivity, can be effectively described in terms of interactions among the fermionic charge carriers mediated by the exchange of bosons. The problem can be rationalized by considering the Hubbard model, in which the instantaneous virtual hopping of holes into already occupied sites (with an energy cost of U) inherently favours an antiferromagnetic (AF) coupling $J = 4t_h^2/U$ between neighbouring sites, where t_h is the nearest-neighbour hopping energy. As a consequence, antiferromagnetic fluctuations with a high-energy cutoff of $2J \ll U$ naturally emerge as a candidate[5] for mediating the low-energy electronic interactions, on a characteristic retarded timescale of the order of $\hbar/2J$.

In principle, time-resolved optical spectroscopy[6] may be used to prove the existence of an effective retarded boson-mediated interaction, provided that the temporal resolution is of the order of the inverse bosonic-fluctuation scale (for example, $\hbar/2J$ for AF fluctuations) and the optical properties are probed over a sufficiently broad frequency range, to extract the dynamics of the electron–boson coupling. Recent advances in ultrafast optical spectroscopy have succeeded in separately fulfilling these requirements. For example, high-temporal-resolution (<15 fs) experiments[7,8] have been carried out to investigate the ultrafast electron dynamics in copper oxides. Unfortunately, these experiments were typically confined to a very narrow range of visible frequencies, which made it difficult to determine the origin of the measured optical signal. In contrast, the ∼100 fs temporal resolution prevented recent broadband (0.5–2 eV) experiments[9] from directly investigating the possible retardation effects of the ultrafast electron–boson interaction.

Here we overcome these limitations by developing a transient reflectivity experiment[10] that combines the use of extremely short light pulses (9–13 fs) with a broad accessible spectral window, extending from the infrared to the visible region (0.75–2.4 eV) (see Methods). The qualitative idea of the experiment is to use an ultrashort light pulse to impulsively increase the kinetic energy of a small fraction of the charge carriers (photo-excited holes) in doped cuprates. A second broadband pulse probes the instantaneous optical scattering rate by inducing boson-assisted optical transitions of the charge carriers in the conduction band. As long as the number

[1]IFN-CNR, Dipartimento di Fisica, Politecnico di Milano, 20133 Milano, Italy. [2]Department of Physics and Arnold Sommerfeld Center for Theoretical Physics, Ludwig-Maximilians-Universität München, D-80333 München, Germany. [3]J. Stefan Institute, 1000 Ljubljana, Slovenia. [4]Institute of Physics, University of Silesia, 40-007 Katowice, Poland. [5]i-LAMP (Interdisciplinary Laboratories for Advanced Materials Physics), Università Cattolica del Sacro Cuore, Brescia I-25121, Italy. [6]Department of Physics, Università degli Studi di Milano, 20133 Milano, Italy. [7]Department of Physics, Università Cattolica del Sacro Cuore, Brescia I-25121, Italy. [8]Department of Physics and Astronomy, University of British Columbia, Vancouver, British Columbia V6T 1Z1, Canada. [9]Quantum Matter Institute, University of British Columbia, Vancouver, British Columbia V6T 1Z4, Canada. [10]Max Planck Institute for Solid State Research, Heisenbergstrasse 1, D-70569 Stuttgart, Germany. [11]Laboratory for Solid State Physics, ETH, 8093 Zürich, Switzerland. [12]Nanoelectronics Research Institute, National Institute of Advanced Industrial Science and Technology, Tsukuba, Ibaraki 305-8568, Japan. [13]School of Physics and Astronomy, University of Minnesota, Minneapolis, Minnesota 55455, USA. [14]CNR-IOM Dipartimento di Fisica, Università di Roma La Sapienza P.le Aldo Moro 2, 00185 Rome, Italy. [15]Department of Physics and Center for Applied Photonics, University of Konstanz, 78457 Konstanz, Germany. [16]CNR-IOM Democritos National Simulation Center and Scuola Internazionale Superiore di Studi Avanzati (SISSA), Via Bonomea 265, 34136 Trieste, Italy. [17]Faculty of Mathematics and Physics, University of Ljubljana, 1000 Ljubljana, Slovenia. †These authors contributed equally to this work. *e-mail: stefano.dalconte@polimi.it; lev.vidmar@lmu.de; claudio.giannetti@unicatt.it

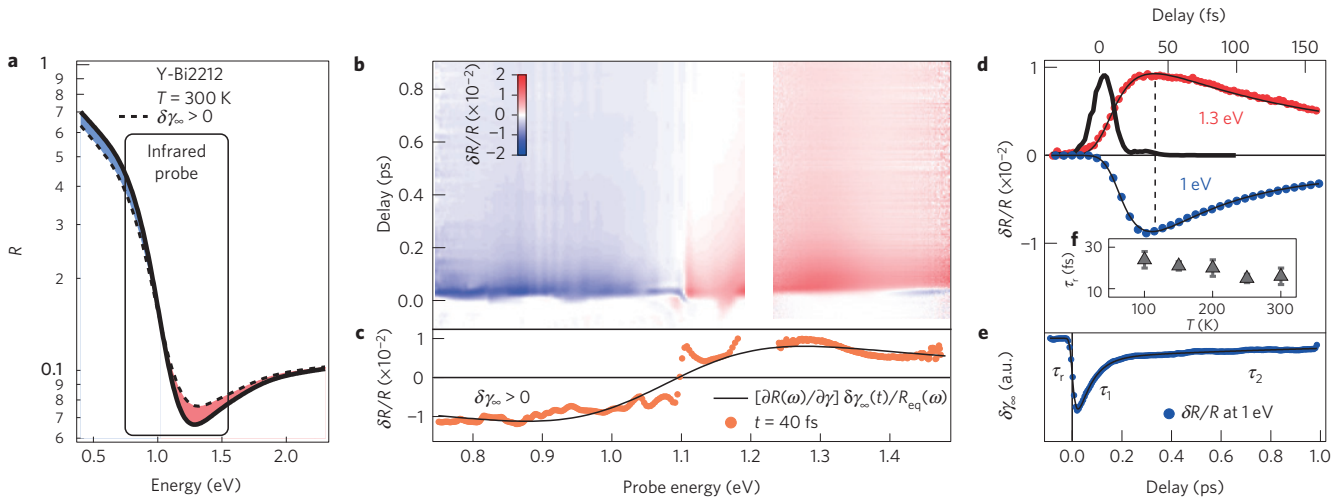

Figure 1 | Equilibrium and non-equilibrium optical properties of Y-Bi2212$_{UD}$ at $T=300$ K. a, The normal state reflectivity (black line) of the Y-Bi2212$_{UD}$ crystal is reported. The dashed line represents the reflectivity calculated by increasing the electron–boson scattering rate, γ_∞, in the extended Drude model. The blue (red) area represents the spectral region in which a negative (positive) reflectivity variation is expected when $\delta\gamma_\infty > 0$. **b**, The ultrafast dynamics of $\delta R/R(\omega,t)$, measured across the isosbestic point $\tilde{\omega}$, is reported. The measurements have been performed with an incident pump fluence of 0.7 mJ cm^{-2}. The linearity of the optical response has been checked in the 0.2–2 mJ cm^{-2} fluence range. **c**, The maximum reflectivity variation at fixed delay, that is, $\delta R(\omega, t=40\,\text{fs})/R_{eq}(\omega)$, is reported as orange dots. Already on this ultrafast timescale the signal can be accurately reproduced by exclusively increasing γ_∞ in the EDM (black line). **d**, Two different time traces at $\hbar\omega=1.3$ eV (red dots) and $\hbar\omega=1$ eV (blue dots) are displayed. The black line is the fit to the data of the function $F(t)=(1-\exp(-t/\tau_r))\times(I_1\exp(-t/\tau_1)+I_2\exp(-t/\tau_2))$ convolved with a Gaussian pulse accounting for the experimental time resolution. The dark-grey line is the measured cross-correlation trace between the pump and probe pulses, which sets the time resolution to 19 ± 2 fs. The temporal width of the cross-correlation is monitored before and after each measurement. The time $t=0$ is defined at the maximum of the pump-probe cross-correlation. The vertical dashed line highlights the time delay (~40 fs), with respect to $t=0$, at which the maximal $\delta\gamma_\infty$ variation is measured. **e**, Picosecond dynamics of the 1.3 eV time trace (blue dots). **f**, Temperature dependence of τ_r. The error bars have been obtained from the fitting of the function $F(t)$ to the time traces reported in Supplementary Fig. 2.

of photo-excited holes is small relative to the intrinsic doping of the system (see Methods), we can assume that we are probing the average scattering rate experienced by the holes which have not been directly excited by the pump pulse. Because the optical scattering rate is proportional to the energy stored in the bosonic fluctuations, we can monitor the time needed to complete the energy exchange from the photo-excited carriers to the bosonic bath.

Quantitatively, the dynamics of the optical scattering rate after the impulsive excitation of a prototypical superconducting cuprate can be retrieved by probing the damping of the infrared plasma edge. This is easily shown by inspection of the room-temperature equilibrium reflectivity, $R_{eq}(\omega)$, of a $Bi_2Sr_2Y_{0.08}Ca_{0.92}Cu_2O_{8+\delta}$ (Y-Bi2212$_{UD}$) crystal[11]. The doping level (hole concentration $p\simeq0.13$, $T_c\simeq89$ K) is close to optimal ($p\simeq0.16$, $T_c\simeq96$ K), and we estimate the opening of the pseudogap to occur at $T^*\simeq240$ K (ref. 12). As shown in Fig. 1a, the infrared region is dominated by a broad plasma edge, which can be effectively reproduced by an extended Drude model (EDM; ref. 13) described by $4\pi\sigma_D(\omega)=\omega_p^2/[\gamma(\omega,T)-i\omega(1+\tilde{\lambda}(\omega,T))]$, where $\sigma_D(\omega)$ is the EDM optical conductivity, ω_p the plasma frequency and $1+\tilde{\lambda}$ the renormalization factor of the effective mass of the carriers. The optical scattering rate, $\gamma(\omega,T)$, controls the damping of the plasma edge and it is, in principle, a function of the frequency and temperature, as a consequence of the coupling to bosonic fluctuations whose occupation number is regulated by Bose–Einstein statistics[13]. Nevertheless, in the energy window probed in the experiment, $\gamma(\omega,T)$ varies by less than 10% as a function of frequency (see Supplementary Information), therefore we can safely discuss the time-resolved results considering its asymptotic ($\omega\to\infty$) value, that is, $\gamma_\infty(T)$. If the total scattering rate is enhanced ($\delta\gamma_\infty>0$) by any effect, this leads to a further damping of the edge and to the evolution of $R_{eq}(\omega)$ shown in Fig. 1a. An isosbestic point is found at the frequency $\tilde{\omega}\simeq1.1$ eV, across which the reflectivity variation changes from negative to positive.

In Fig. 1b we report the dynamics of the relative reflectivity variation, $\delta R(\omega,t)/R_{eq}(\omega)$, measured at $T=300$ K on Y-Bi2212$_{UD}$ as a function of the delay t between the pump and probe pulses. The sub-10 fs pump pulse is set to 2.1 eV central energy, to avoid the spurious signals measured when pumping below the Drude absorption edge[14]. The probe spans the energy range across $\tilde{\omega}$, which is more sensitive to the possible variations of $\gamma_\infty(T)$, as already shown in Fig. 1a. One key result of this experiment is that, for each given time delay t from the very first femtoseconds up to the picosecond timescale, $\delta R(\omega,t)/R_{eq}(\omega)$ can be reproduced very well by exclusively increasing γ_∞. This is shown in Fig. 1c, which shows the relative reflectivity variation at the fixed delay time $t=40$ fs. The signal is accurately reproduced over the entire accessible frequency range by assuming a small increment $\delta\gamma_\infty$—that is, $\delta R(\omega,t)/R_{eq}(\omega)=[\partial R(\omega)/\partial\gamma]\,\delta\gamma_\infty(t)/R_{eq}(\omega)$. In other words, already on the sub-100 fs timescale the variation of the optical properties is dominated by the change of the electron–boson scattering rate, as a consequence of the ultrafast increase in the average energy stored in the boson bath. We point out that a dominant direct interaction—that is, unmediated by the boson bath—of the photo-excited holes with the other existing holes would lead to an increase of the effective electronic temperature, T_e, decoupled from the boson temperature, $T_b\simeq T$. However, an increase of T_e alone would provide a qualitatively different $\delta R(\omega,t)/R_{eq}(\omega)$ signal, as discussed in ref. 9 (see also Supplementary Information). Bringing together all these observations, we can assume a direct proportionality between the reflectivity variation at a fixed frequency and the electron–boson scattering rate change, that is, $\delta R(t)\propto\delta\gamma_\infty(t)$.

The inherent timescale of the electron–boson interaction can be thus accessed by plotting the $\delta R(t)/R_{eq}$ time traces. In particular, in Fig. 1d we report two different time traces across the isosbestic frequency $\tilde{\omega}$, at $\hbar\omega=1.3$ and 1 eV. Although opposite in sign, in both cases the maximum variation of $\delta R(t)/R_{eq}$ is measured at a non-zero

delay time (∼40 fs) from the excitation, as shown in Fig. 1d. The build-up time of the $\delta R(t)/R_{eq}$ signal ($\tau_r = 16 \pm 3$ fs) is extracted by fitting the dynamics with the simple function $(1-\exp(-t/\tau_r)) \times (I_1 \exp(-t/\tau_1) + I_2 \exp(-t/\tau_2))$ convolved with a Gaussian pulse accounting for the experimental resolution (pump–probe cross-correlation with a full-width at half-maximum of 19 ± 2 fs), which has been carefully checked through the cross frequency-resolved optical gating method (see Supplementary Information). This result demonstrates that the energy exchange between the photo-excited holes and the boson bath, which ultimately leads to the measured increase of $\gamma_\infty(t)$, builds up with a non-zero time constant of the order of 15–20 fs. The two further decay scales ($\tau_1 \sim 90$ fs and $\tau_2 \sim 1$ ps), measured in the $\delta R(t)/R_{eq}$ signal shown in Fig. 1e, are related to the subsequent coupling with the optical buckling and breathing phonons (τ_1) and with the rest of the lattice vibrations (τ_2; refs 7,9,15). Remarkably, any time trace in the whole probed frequency range exhibits the same values of τ_r, τ_1 and τ_2. Similar results are obtained by performing a quantitative and global analysis[16,17] through singular value decomposition (see Supplementary Information), which provides the global dynamics $\delta\gamma_\infty(t)$ under the form of the first temporal eigenvector.

The present high-time-resolution transient reflectivity experiment demonstrates that the electron dynamics in the hole-doped cuprates can be captured by an effective model in which the charge carriers exchange energy with bosonic excitations on a very fast (but non-zero) timescale. This conclusion is based solely on the observation that $\delta R(t)$ is proportional to $\delta\gamma_\infty(t)$—that is, to the total energy stored in the boson bath—and does not necessarily require an effective thermalization of the charge carriers through direct carrier–carrier collisions[18].

Considering that the elementary time ($\hbar/t_h \sim 2$ fs) associated with the Cu–O–Cu hole-hopping process inevitably leads to the creation of local AF excitations, AF fluctuations are a candidate as the dominant mediators of the hole interactions on this ultrafast timescale. As further support of our assignment, neutron and X-ray scattering experiments[19–24] have revealed a rich magnetic dynamics in hole-doped cuprates, characterized by resonance modes at 50–60 meV and a very broad spectrum with a cutoff of the order of the bandwidth $2J \simeq 240$ meV found for the AF parent compounds. Similar bosonic-fluctuation spectra have been extracted from equilibrium optical spectroscopy[13]. On the other hand, we can rule out a possible photo-induced coherent rearrangement of the oxygen atoms, which has been demonstrated on the 18 fs timescale[25] because no significant variation of the charge transfer excitations (∼2 eV), which are the most sensitive to a rearrangement of the oxygen orbitals, is observed (see Supplementary Information) and no coherent oscillation is detected in the $\delta R(\omega,t)/R_{eq}(\omega)$ signal at any wavelength. Even though a single incoherent scattering process with optical phonons could be extremely fast, several scattering processes are necessary to complete the energy transfer to the phonons, as will be shown later in the case of the conventional superconductor MgB_2. Finally, in the scenario of an ultrafast coupling between charge carriers and bosonic excitations, such as AF fluctuations, the dynamics of the energy exchange should be regulated by the strength of the electron–boson coupling and the boson energy spectrum. Therefore, the dynamics should be essentially independent of temperature, at least for temperatures lower than the typical boson frequency. To verify this hypothesis, we performed measurements of τ_r at different base temperatures of the Y-Bi2212$_{UD}$ sample, the results of which are reported in Fig. 1f. Within the error bars, a constant value of τ_r is measured over a broad temperature range. This result supports the possibility of defining a unique ultrafast timescale, determined by the nature of the bosonic mediators of the charge dynamics.

The role of short-range AF correlations as the fastest effective bosons mediating the charge dynamics is corroborated by studying

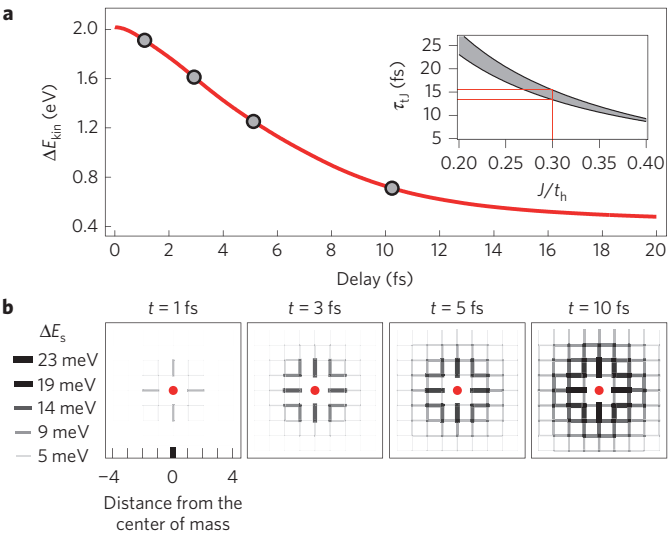

Figure 2 | Microscopic calculation of the energy transfer from a photo-excited hole to local antiferromagnetic bonds through the out-of-equilibrium t–J model (see Methods for further details). **a**, Time evolution of the hole kinetic energy variation, $\Delta E_{kin}(t)$. In the main panel we set $J/t_h = 0.3$, where $t_h = 360$ meV represents the hopping amplitude. The inset shows the range of the characteristic relaxation time τ_{tJ} at different values of J/t_h, after a finite-size scaling (see Supplementary Information). **b**, Snapshots of the relative energy increase of the local antiferromagnetic bonds $\Delta E_s(t,\mathbf{r})$ on a 9 × 9 square lattice around the photo-excited hole (red circle). The thickness of the black segments is proportional to the energy stored in each bond. The grey dots in **a** indicate the delay times of the snapshots in **b**.

the non-equilibrium dynamics of the photo-excited holes in the t–J Hamiltonian[26,27] (see Methods), which is the minimal model that fully retains the dynamics at the energy scale J. As the rate of the photo-excitation of holes in the system is very low (see Methods), we conjecture that the key relaxation mechanism at very short times corresponds to the creation of high-energy AF excitations in the proximity of the photo-excited holes. We model the photo-excitation of a hole immersed in the AF background by instantaneously raising its kinetic energy, by $\Delta E_{kin}(t) = 2$ eV. The relaxation dynamics is calculated by numerically integrating the time-dependent Schrödinger equation, without any assumption of quasi-thermal intermediate states, as usually described by effective electronic and bosonic temperatures. The dynamics of $\Delta E_{kin}(t)$ after the quench is reported in Fig. 2a. Although the total energy remains constant during the time evolution, the observed relaxation of $\Delta E_{kin}(t)$ is compensated by the simultaneous increase of the energy stored in the AF background. Figure 2b shows snapshots of the excess antiferromagnetic energy density, $\Delta E_s(t,\mathbf{r})$, in the vicinity of the photo-excited hole. We note that the excitation process involves predominantly the neighbouring bonds, demonstrating that short-range AF correlations are sufficient for describing the relaxation dynamics. The characteristic relaxation time, τ_{tJ}, of the energy transfer to AF fluctuations is governed by the ratio J/t_h, as shown in the inset of Fig. 2a. Setting $J/t_h = 0.3$ to a realistic value and performing a finite-size scaling analysis (see Supplementary Information), we obtain $\tau_{tJ} \sim 15$ fs, which is in excellent quantitative agreement with the experimental observations. This value is several times the elementary timescale ($\hbar/t_h \sim 2$ fs) of a single hopping event creating a local AF excitation. To complete the energy exchange process, many events are necessary, each releasing a fraction of J of energy. Consequently, the maximum number of AF excitations, which results in the measured increase of $\delta\gamma_\infty(t)$, is observed when

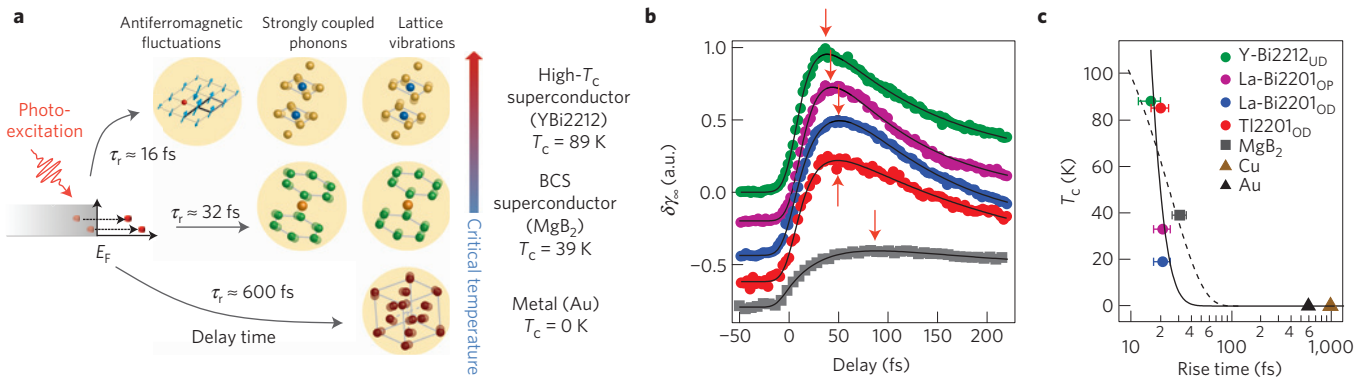

Figure 3 | Ultrafast dynamics of the electron–boson interaction. a, The different relaxation dynamics in a high-T_c superconductor and in conventional superconductors are sketched on the left. **b**, The dynamics of $\delta\gamma_\infty(t)$ are shown for different superconducting systems (Y-Bi2212$_{UD}$, green circles; La-Bi2201$_{OP}$, purple circles; La-Bi2201$_{OD}$, blue circles; Tl2201$_{OD}$, red circles; MgB_2, grey squares). The red arrows highlight the time delay corresponding to the maximal value of $\delta\gamma_\infty(t)$ after the excitation. Note that the maximal value of $\delta\gamma_\infty(t)$ does not necessarily coincide with the τ_r build-up time, which is estimated by fitting three exponential dynamics to the data, as explained in the text. **c**, Critical temperatures of the systems considered, reported as a function of the build-up time (τ_r) of $\delta\gamma_\infty(t)$, measured through time-resolved optical spectroscopy. The black line is the critical temperature calculated by the Eliashberg-like expression $k_B T_c = 0.83\tilde{\Omega}\exp\{[-1.04(1+\lambda_b)]/[\lambda_b - \mu^*(1+0.62\lambda_b)]\}$ (ref. 32), fixing $\mu^* = 0$ and assuming a generic relation between the electron–boson energy exchange rate, $1/\tau_r$, in cuprates and the total coupling constant, λ_b, and $\tilde{\Omega} = 300$ meV (solid line). The dashed line represents the critical temperatures calculated for $\tilde{\Omega} = 50$ meV, $\mu^* = 0.17$ and $\lambda_b = 1.1$ compatible with the phonon-mediated pairing in MgB_2 (ref. 29).

the relaxation is completed—that is, with a delay of about 15 fs. This extremely fast dynamics has been confirmed by very recent non-equilibrium dynamical mean field theory (DMFT) calculations[28]. We remark that the value of τ_{tJ} is not significantly altered when the direct charge–charge interaction between two holes is considered (see Supplementary Information) by a adding an explicit interaction term to the t–J Hamiltonian. We stress that, even in the picture of a boson-mediated relaxation, U is the crucial interaction because it determines the dynamics through the strength of the ferromagnetic coupling, $J = 4t_h^2/U$. This is further discussed in the Supplementary Methods by analysing DMFT calculations for the Hubbard model at finite temperature and doping.

Finally, valuable insight into the general relation between the electron–boson coupling and the dynamics of $\delta\gamma_\infty(t)$ is provided by the results obtained on different families of cuprates and on more conventional superconductors (see Fig. 3). We repeated the same experiment on optimally doped (La–Bi2201$_{OP}$, $T_c = 33$ K) and overdoped (La–Bi2201$_{OD}$, $T_c = 19$ K) single Cu–O layer $Bi_2Sr_{2-x}La_xCuO_6$ crystals, and on slightly overdoped (Tl2201$_{OD}$, $T_c = 88$ K) $Tl_2Ba_2CuO_{6+\delta}$ crystals. The time necessary to attain the maximal variation of γ_∞ is non-zero ($\tau_r = 21 \pm 4$ fs for La–Bi2201$_{OP}$, $\tau_r = 22 \pm 4$ fs for La–Bi2201$_{OD}$ and $\tau_r = 20 \pm 4$ fs for Tl2201$_{OD}$), slightly longer than for Y-Bi2212$_{UD}$. These results demonstrate that the coupling to bosonic fluctuations on the ultrafast timescale is a general property of the normal state of hole-doped cuprates even at large hole-doping concentrations. Qualitatively different results are obtained on MgB_2, which is considered the conventional phonon-mediated superconducting system with the highest critical temperature ($T_c = 39$ K). Here, the maximum variation of the scattering rate after the impulsive excitation is significantly delayed (~90 fs, as shown in Fig. 3b) and $\tau_r = 32 \pm 3$ fs is measured. This result demonstrates that, in the systems in which the superconducting pairing is mediated by high-energy ($\omega_0 \sim 70$ meV) optical phonons[29], the electron–phonon energy exchange process is completed on a timescale that is several times the inverse energy of the phonons involved. Furthermore, a single slower exponential decay ($\tau_1 = 500$ fs) is measured in the $\delta R(\omega, t)$ signal of MgB_2, corresponding to the energy exchange with the rest of the lattice. On conventional non-superconducting metals, such as Cu and Au, time-resolved measurements have been widely applied[30,31], evidencing an electron–phonon coupling on the order of ~600 fs in Au and ~1 ps in Cu. Figure 3c summarizes all the results obtained in both conventional and unconventional superconductors, demonstrating a universal relation between the energy of the boson modes mediating the electron interactions in the normal state and the timescale of the dynamics of the electron–boson scattering rate after the pump excitation. Intriguingly, the dependence of the critical temperature of the system on the experimental τ_r follows the general and qualitative trend of the approximate solution of McMillan's equation[32]. This fact supports a direct relation[33] (or, at least, a strong statistical correlation) between the measured $1/\tau_r$ and the total coupling constant $\lambda_b = 2\int \Pi(\Omega)/\Omega d\Omega$, where $\Pi(\Omega)$ is the coupling function to antiferromagnetic fluctuations ($I^2\chi(\Omega)$) for copper oxides and to phonons ($\alpha^2F(\Omega)$) for MgB_2 and metals.

Methods

Experimental set-up. A Ti:sapphire amplifier (Clark-MXR model CPA-1) delivers a train of pulses at a 1 kHz repetition rate with a duration of 150 fs at a central wavelength of 780 nm and is used to simultaneously drive three non-collinear optical parametric amplifiers (NOPAs) operating in different frequency intervals. All NOPAs are seeded by a white light continuum (WLC) generated in a sapphire plate. The first NOPA (NOPA1) is pumped by the fundamental wavelength and is amplified by fulfilling a quasi-phase-matching condition in a periodically poled stoichiometric $LiTaO_3$ (PPSLT) crystal. The signal generated in this process covers a spectral range between 1 μm (1.24 eV) and 1.5 μm (0.83 eV) and is temporally compressed to a nearly transform-limited pulse duration (8.5 fs) by a deformable-mirror-based pulse shaper[34]. The second NOPA (NOPA2) is pumped by the second harmonic and is amplified in a beta-barium borate (BBO) crystal pulses with a spectral content between 820 nm (1.5 eV) and 1,050 nm (1.2 eV), which are compressed to a nearly transform-limited 13 fs duration by a pair of fused silica prisms. Both these NOPAs serve to probe the transient response of the sample and are synchronized with a third NOPA (NOPA3), pumped by the second harmonic and using BBO, which initiates the dynamics. The spectrum of NOPA3 spans a frequency range between 510 nm (2.4 eV) and 700 nm (1.8 eV) and it is compressed to a 7 fs duration by multiple reflections between a pair of chirped mirrors, giving an overall temporal resolution of the pump–probe set-up below 19 fs. The time delay between pump and probe is adjusted by a motorized delay stage and both the beams are focused on the sample by a spherical mirror in a quasi-collinear geometry. The spectra of the NOPA1 and NOPA2 probes are detected respectively by InGaAs and Si spectrometers working at the full 1 kHz laser repetition rate. By recording the reflected probe spectra at different temporal delays t with and without pump excitation, we measure the differential reflectivity: $\delta R(\omega,t)/R_{eq}(\omega) = [R(\omega,t) - R_{eq}(\omega)]/R_{eq}(\omega)$. The low-temperature measurements have been performed in a cryostat equipped with a very thin

(200 μm) fused silica optical window, to avoid any significant temporal broadening of the pump and probe pulses.

Samples. The Y-substituted Bi2212 single crystals were grown[11] in an image furnace using the travelling solvent floating-zone technique with a non-zero Y content to maximize T_c. The underdoped samples were annealed at 550 °C for 12 days in a vacuum-sealed glass ampoule with copper metal inside. All the La–Bi2201 crystals were grown using the floating-zone technique, and characterized as described elsewhere[35]. $Tl2201_{OD}$ single crystals were grown[36] using a copper-rich self-flux method, with stoichiometry $Tl_{1.88(1)}Ba_2Cu_{1.11(2)}O_{6+\delta}$ corresponding to Cu substitution on the Tl site, thus away from the CuO_2 planes. High-quality MgB_2 single crystals were grown using the high-pressure cubic anvil technique[37].

***t*–*J* model out of equilibrium.** We investigate the ultrafast energy exchange between doped fermionic carriers (holes) and short-range antiferromagnetic fluctuations within the *t*–*J* model on a square lattice,

$$H_{tJ} = -t_h \sum_{\langle \mathbf{ij}\rangle,\sigma} (\tilde{c}^{\dagger}_{i,\sigma}\tilde{c}_{j,\sigma}\, e^{i\phi_{i,j}(t)} + \text{H.c.}) + \sum_{\langle \mathbf{ij}\rangle} J\left(\mathbf{S}_i\cdot\mathbf{S}_j - \frac{1}{4}\tilde{n}_i\tilde{n}_j\right) \quad (1)$$

where $\tilde{c}_{i,\sigma} = c_{i,\sigma}(1-n_{i,-\sigma})$ is a projected fermion operator, t_h represents the nearest-neighbour overlap integral, the sum $\langle \mathbf{ij}\rangle$ runs over pairs of nearest neighbours, J is the antiferromagnetic exchange energy, $\mathbf{S}_i$ is the spin vector operator and $\tilde{n}_i = n_{i,\uparrow} + n_{i,\downarrow} - 2n_{i,\uparrow}n_{i,\downarrow}$ is a projected electron number operator. The system is threaded by a time-dependent flux $\phi_{i,j}(t)$, which induces the electric field $-\partial_t\phi_{i,j}(t)$.

Motivated by the experimental results, we model the dynamics far from equilibrium under the following two assumptions. First, we mimic the effect of an ultrashort laser pump pulse by instantly increasing the kinetic energy of a doped carrier, while the chargeless spin degrees of freedom remain unchanged. In the context of the *t*–*J* model in equation (1), we first calculate the ground state with $\phi_{i,j}=0$, then we perform a sudden change (quench) of the phase at time $t=0$, describing the δ-like pulse of the electric field. Such a phase quench is obtained by setting $\phi_{i,i+\mathbf{e}_{x(y)}}(t) = \pi\theta(t)$, where $\mathbf{e}_{x(y)}$ represents the lattice vector in the $x(y)$-direction. Second, in a generic situation, promptly after the absorption of the pump pulse, the kinetic energy of only a fraction of holes (also referred to as photo-excited holes) is suddenly increased. For optimally doped samples ($p\sim0.16$) and a pump pulse with photon energy 2 eV, fluence 700 μJ cm^{-2} and penetration depth 170 nm, the doping rate representing photo-excited holes is rather low, $p_0\sim0.01$, assuming that each photo-excited hole absorbs an entire quantum of light, that is, 2 eV. We therefore study the dynamics of a single photo-excited hole, assuming that the main relaxation mechanism is represented by coupling of the photo-excited hole to local antiferromagnetic excitations. As a consequence of finite chemical and photo doping, the average number of antiferromagnetic bonds that are available to absorb the excess kinetic energy of a single photo-excited hole is large but finite. Although our method is limited to the calculation of single-hole dynamics, we simulate the effect of small photo doping by limiting the propagation of the photo-excited hole to a finite $L\times L$ plaquette with $L<10$.

Because exact diagonalization (ED) is limited to clusters which are too small to account for the complete relaxation within the experimental conditions described above, we extend the lattice size by employing diagonalization in a limited functional space. The latter method was recently successfully applied to describe non-equilibrium properties of a charge carrier propagating in a local antiferromagnetic background[26,27]. The advantage of this method over the standard ED in the equilibrium regime follows from a systematic construction of states with distinct configurations of local antiferromagnetic excitations in the proximity of the hole. In addition, it remains efficient even when applied to non-equilibrium systems on short and intermediate timescales, as long as the antiferromagnetic disturbance caused by the local quench remains within the boundaries of generated excitations[26,27]. We first construct the parent state

$$|\varphi^{(0)}\rangle = c_{\mathbf{k},\sigma}|\text{Néel}\rangle$$

which represents a hole with momentum $\mathbf{k}$, doped into the Néel state. The functional space[38] is then generated by

$$\left\{|\varphi_j^{(n_h)}\rangle\right\} = \left[H_{\text{kin}} + \tilde{H}_J\right]^{n_h}|\varphi^{(0)}\rangle, n_h = 0,\ldots,N_h$$

where H_{kin} represents the kinetic energy term of the *t*–*J* model and $\tilde{H}_J$ represents the spin-flip term of the Heisenberg part of the *t*–*J* model (spin-flip denotes overturned spins with respect to the Néel state; $\tilde{H}_J$ erases two neighbouring spin-flips created by the propagating hole). The size of the functional space is determined by the parameter N_h. In addition, we impose the condition that the largest distance of a local antiferromagnetic excitation away from the photo-excited hole, $\tilde{\mathbf{r}} = (N_{\text{box}}, N_{\text{box}})$, should not exceed $N_{\text{box}}=4$, therefore limiting the spatial extent of antiferromagnetic excitations to a 9×9 plaquette. Contrary to the standard ED, we carry out a finite-size scaling not with respect to the geometric size of the system, but rather with respect to N_h (see Supplementary Information).

Applying the Lanczos technique we first compute the ground state $|\Psi(t=0)\rangle$. The time evolution $|\Psi(t)\rangle = e^{-iH_{tJ}t/\hbar}|\Psi(t=0)\rangle$ is then implemented using the quenched Hamiltonian. We set the hopping amplitude $t_h = 0.360$ eV, which corresponds to the time unit $\hbar/t_h = 1.83$ fs. At each time step $\delta t(t_h/\hbar) \ll 1$ we generate the evolution $|\Psi(t-\delta t)\rangle \to |\Psi(t)\rangle$ by using the Lanczos basis[39]. We measure in Fig. 2a the time-dependent expectation value of the kinetic energy relative to the initial state, $\Delta E_{\text{kin}}(t) = E_{\text{kin}}(t) - E^{(0)}_{\text{kin}}$, where $E_{\text{kin}}(t) = \langle H_{\text{kin}}(t)\rangle$ and $E^{(0)}_{\text{kin}} = \langle H_{\text{kin}}(t<0)\rangle$. In Fig. 2b we plot the relative increase of the spin energy on the antiferromagnetic bond at a distance $\mathbf{r}$ away from the photo-excited hole, $\Delta E_s(t,\mathbf{r}) = E_s(t,\mathbf{r}) - E^{(0)}_s(\mathbf{r})$, where $E_s(t,\mathbf{r}) = J\langle \mathbf{S}_{i+\mathbf{r}}(t)\cdot\mathbf{S}_{j+\mathbf{r}}(t)\rangle$ and $E^{(0)}_s(\mathbf{r}) = J\langle \mathbf{S}_{i+\mathbf{r}}(t<0)\cdot\mathbf{S}_{j+\mathbf{r}}(t<0)\rangle$. After the quench, the total energy in the system remains constant, $\Delta E_{\text{kin}}(t) + \sum_{\mathbf{r}}\Delta E_s(t,\mathbf{r}) = \text{const}$.

Received 10 February 2014; accepted 28 January 2015; published online 9 March 2015

References

1. Lee, P. A., Nagaosa, N. & Wen, X-G. Doping a Mott insulator: Physics of high-temperature superconductivity. *Rev. Mod. Phys.* **78,** 17–85 (2006).
2. Anderson, P. W. Is there glue in cuprate superconductors? *Science* **316,** 1705–1707 (2007).
3. Scalapino, D. J. A common thread: The pairing interaction for unconventional superconductors. *Rev. Mod. Phys.* **84,** 1383–1417 (2012).
4. Monthoux, P., Pines, D. & Lonzarich, G. G. Superconductivity without phonons. *Nature* **450,** 1177–1183 (2007).
5. Gull, E. & Millis, A. J. Pairing glue in the two-dimensional Hubbard model. *Phys. Rev. B* **90,** 041110 (2014).
6. Orenstein, J. Ultrafast spectroscopy in quantum materials. *Phys. Today* **65**(9), 44–50 (2012).
7. Gadermaier, C. *et al.* Electron–phonon coupling in high-temperature cuprate superconductors determined from electron relaxation rates. *Phys. Rev. Lett.* **105,** 257001 (2010).
8. Gadermaier, C. *et al.* Strain-induced enhancement of the electron energy relaxation in strongly correlated superconductors. *Phys. Rev. X* **4,** 011056 (2014).
9. Dal Conte, S. *et al.* Disentangling the electronic and phononic glue in a high-T_c superconductor. *Science* **335,** 1600–1603 (2012).
10. Brida, D. *et al.* Few-optical-cycle pulses tunable from the visible to the mid-infrared by optical parametric amplifiers. *J. Opt.* **12,** 013001 (2010).
11. Eisaki, H. *et al.* Effect of chemical inhomogeneity in bismuth-based copper oxide superconductors. *Phys. Rev. B* **69,** 064512 (2004).
12. Cilento, F. *et al.* Photo-enhanced antinodal conductivity in the pseudogap state of high-T_c cuprates. *Nature Commun.* **5,** 4353 (2014).
13. Van Heumen, E. *et al.* Optical determination of the relation between the electron–boson coupling function and the critical temperature in high-T_c cuprates. *Phys. Rev. B* **79,** 184512 (2009).
14. Novelli, F. *et al.* Witnessing the formation and relaxation of dressed quasi-particles in a strongly correlated electron system. *Nature Commun.* **5,** 5112 (2014).
15. Perfetti, L. *et al.* Ultrafast electron relaxation in superconducting $Bi_2Sr_2CaCu_2O_{8+\delta}$ by time-resolved photoelectron spectroscopy. *Phys. Rev. Lett.* **99,** 197001 (2007).
16. Kaindl, R. A. *et al.* Ultrafast mid-infrared response of $YBa_2Cu_3O_{7-\delta}$. *Science* **287,** 470–473 (2000).
17. Coslovich, G. *et al.* Competition between the pseudogap and superconducting states of $Bi_2Sr_2Ca_{0.92}Y_{0.08}Cu_2O_{8+\delta}$ single crystals revealed by ultrafast broadband optical reflectivity. *Phys. Rev. Lett.* **110,** 107003 (2013).
18. Baranov, V. V. & Kabanov, V. V. Theory of electronic relaxation in a metal excited by an ultrashort optical pump. *Phys. Rev. B* **89,** 125102 (2014).
19. Dahm, T. *et al.* Strength of the spin-fluctuation-mediated pairing interaction in a high-temperature superconductor. *Nature Phys.* **5,** 217–221 (2009).
20. Le Tacon, M. *et al.* Intense paramagnon excitations in a large family of high-temperature superconductors. *Nature Phys.* **7,** 725–730 (2011).
21. Fujita, M. *et al.* Progress in neutron scattering studies of spin excitations in high-T_c cuprates. *J. Phys. Soc. Jpn* **81,** 011007 (2012).
22. Dean, M. P. M. *et al.* High-energy magnetic excitations in the cuprate superconductor $Bi_2Sr_2CaCu_2O_8$: Towards a unified description of its electronic and magnetic degrees of freedom. *Phys. Rev. Lett.* **110,** 147001 (2013).
23. Le Tacon, M. *et al.* Dispersive spin excitations in highly overdoped cuprates revealed by resonant inelastic X-ray scattering. *Phys. Rev. B* **88,** 020501 (2013).

24. Dean, M. P. M. *et al.* Persistence of magnetic excitations in $La_{2-x}Sr_xCuO_4$ from the undoped insulator to the heavily overdoped non-superconducting metal. *Nature Mater.* **12,** 1019–1023 (2013).
25. Singla, R. *et al.* Photoinduced melting of the orbital order in $La_{0.5}Sr_{1.5}MnO_4$ measured with 4-fs laser pulses. *Phys. Rev. B* **88,** 075107 (2013).
26. Mierzejewski, M., Vidmar, L., Bonča, J. & Prelovšek, P. Nonequilibrium quantum dynamics of a charge carrier doped into a Mott insulator. *Phys. Rev. Lett.* **106,** 196401 (2011).
27. Golež, D., Bonča, J., Mierzejewski, M. & Vidmar, L. Mechanism of ultrafast relaxation of a photo-carrier in antiferromagnetic spin background. *Phys. Rev. B* **89,** 165118 (2014).
28. Eckstein, M. & Werner, P. Ultra-fast photo-carrier relaxation in Mott insulators with short-range spin correlations. Preprint at http://arxiv.org/abs/1410.3956 (2014).
29. Kong, Y., Dolgov, O. V., Jepsen, O. & Andersen, O. K. Electron–phonon interaction in the normal and superconducting states of MgB_2. *Phys. Rev. B* **64,** 020501 (2001).
30. Della Valle, G., Conforti, M., Longhi, S., Cerullo, G. & Brida, D. Real-time optical mapping of the dynamics of nonthermal electrons in thin gold films. *Phys. Rev. B* **86,** 155139 (2012).
31. Elsayed-Ali, H. E., Norris, T. B., Pessot, M. A. & Mourou, G. A. Time-resolved observation of electron-phonon relaxation in copper. *Phys. Rev. B* **58,** 1212–1215 (1987).
32. Allen, P. B. & Dynes, R. C. Transition temperature of strong-coupled superconductors reanalyzed. *Phys. Rev. B* **12,** 905–922 (1975).
33. Allen, P. B. Theory of thermal relaxation of electrons in metals. *Phys. Rev. Lett.* **59,** 1460–1463 (1987).
34. Brida, D. *et al.* Generation of 8.5 fs pulses at 1.3 μm for ultrabroadband pump–probe spectroscopy. *Opt. Express* **17,** 12510 (2009).
35. Ono, S. & Ando, Y. Evolution of the resistivity anisotropy in $Bi_2Sr_{2-x}La_xCuO_{6+\delta}$ single crystals for a wide range of hole doping. *Phys. Rev. B* **67,** 104512 (2003).
36. Peets, D. C. *et al.* $Tl_2Ba_2CuO_{6+\delta}$ brings spectroscopic probes deep into the overdoped regime of the high-T_c cuprates. *New J. Phys.* **9,** 28 (2007).
37. Zhigadlo, N. D. *et al.* Influence of Mg deficiency on crystal structure and superconducting properties in MgB_2 single crystals. *Phys. Rev. B* **81,** 054520 (2010).
38. Bonča, J., Maekawa, S. & Tohyama, T. Numerical approach to the low-doping regime of the t–J model. *Phys. Rev. B* **76,** 035121 (2007).
39. Park, T. J. & Light, J. C. Unitary quantum time evolution by iterative Lanczos reduction. *J. Chem. Phys.* **85,** 5870–5876 (1986).

Acknowledgements

We thank F. Cilento, G. Coslovich, D. Fausti, F. Parmigiani, D. Mihailović, P. Prelovšek, V.V. Kabanov, U. Bovensiepen, M. Eckstein, A. Avella, D. van der Marel, L. Boeri, L. de' Medici, A. Cavalleri, D. Manske, B. Keimer and D.J. Scalapino for useful and fruitful discussions. We gratefully acknowledge D. Bonn and B. Keimer for support in the development of the MPI-UBC $Tl2201_{OD}$ research effort. The research activities of S.D.C., F.B, G.F., M.C. and C.G. received funding from the European Union, Seventh Framework Programme (FP7 2007-2013), under Grant No. 280555 (GO FAST). S.D.C. received financial support from Futuro through Ricerca grant No. RBFR12SW0J of the Italian Ministry of Education, University and Research. L.V. is supported by the Alexander von Humboldt Foundation. M.M. acknowledges support from the DEC-2013/09/B/ST3/01659 project of the Polish National Science Center. The $Y\text{-}Bi2212_{UD}$ crystal growth work was performed in M.G.'s previous laboratory at Stanford University, Stanford, CA 94305, USA, and supported by the US Department of Energy, Office of Basic Energy Sciences. The work at UBC was supported by the Max Planck—UBC Centre for Quantum Materials, the Killam, A. P. Sloan, Alexander von Humboldt, and NSERC's Steacie Memorial Fellowships (A.D.), the Canada Research Chairs Program (A.D.), NSERC, CFI, and CIFAR Quantum Materials. M.C. is financed by the European Research Council through FP7/ERC Starting Grant SUPERBAD, Grant Agreement 240524. J.B. acknowledges support by the P1-0044 of ARRS, Slovenia and Center for Integrated Nanotechnologies, a US Department of Energy, Office of Basic Energy Sciences user facility. G.C. acknowledges support by the EC under Graphene Flagship (contract no. CNECT-ICT-604391). N.D.Z. acknowledges support from the NCCR project 'Materials with Novel Electronic Properties' and appreciates expert collaboration with J. Karpinski.

Author contributions

C.G., S.D.C. and G.C. conceived the experiments. L.V., M.M. and J.B. conceived the out-of-equilibrium calculations. C.G. coordinated the research activities with input from all the coauthors, in particular S.D.C., L.V., J.B., M.M., M.C., A.D. and G.C. The broadband pump–probe set-up was designed and developed by D.B. and G.C. The time-resolved optical measurements were performed by S.D.C., G.S., S.P., L.C., D.B. and G.C. The analysis of the time-resolved data was performed by S.D.C. and C.G. The out-of-equilibrium t–J model calculations were performed by L.V., D.G., M.M. and J.B. The DMFT calculations were carried out by M.C. The Y-Bi2212 crystals were grown and characterized by H.E., M.G., R.C. and A.D. The Tl-2201 crystals were grown and characterized by L.C. The characterization and measurement of the equilibrium optical properties of the Bi2201 crystals were performed by S.L. The MgB_2 crystals were grown by N.D.Z. and characterized by B.M.L. and N.D.Z. The text was written by C.G. with major input from S.D.C., L.V., M.M., J.B., F.B., G.F., M.G., S.L., M.G., M.C., A.D., D.B. and G.C. All authors extensively discussed the results and the interpretation and revised the manuscript.

Additional information

Supplementary information is available in the online version of the paper. Reprints and permissions information is available online at www.nature.com/reprints. Correspondence and requests for materials should be addressed to S.D.C., L.V. or C.G.

Competing financial interests

The authors declare no competing financial interests.